



Hydrogen Oxidation Artifact During Platinum Oxide Reduction in Cyclic Voltammetry Analysis of Low-Loaded PEMFC Electrodes

S. Prass¹ · J. St-Pierre² · M. Klingele¹ · K. A. Friedrich^{3,4} · N. Zamel¹

Accepted: 12 October 2020 / Published online: 31 October 2020
© The Author(s) 2020

Abstract

An artifact appearing during the cathodic transient of cyclic voltammograms (CVs) of low-loaded platinum on carbon (Pt/C) electrodes in proton exchange membrane fuel cells (PEMFCs) was examined. The artifact appears as an oxidation peak overlapping the reduction peak associated to the reduction of platinum oxide (PtOx). By varying the nitrogen (N₂) purge in the working electrode (WE), gas pressures in working and counter electrode, upper potential limits and scan rates of the CVs, the artifact magnitude and potential window could be manipulated. From the results, the artifact is assigned to crossover hydrogen (H_{2X}) accumulating in the WE, once the electrode is passivated towards hydrogen oxidation reaction (HOR) due to PtOx coverage. During the cathodic CV transient, PtOx is reduced and HOR spontaneously occurs with the accumulated H_{2X}, resulting in the overlap of the PtOx reduction with the oxidation peak. This feature is expected to occur predominantly in CV analysis of low-loaded electrodes made of catalyst material, whose oxide is inactive towards HOR. Further, it is only measurable while the N₂ purge of the WE is switched off during the CV measurement. For higher loaded electrodes, the artifact is not observed as the electrocatalysts are not fully inactivated towards HOR due to incomplete oxide coverage, and/or the currents associated with the oxide reduction are much larger than the spontaneous HOR of accumulated H_{2X}. However, owing to the forecasted reduction in noble metal loadings of catalyst in PEMFCs, this artifact is expected to be observed more often in the future.

Keywords Cyclic voltammetry · Oxidation artifact · Platinum electrode · Low loading · Hydrogen crossover

Introduction

Cyclic voltammetry (CV) analysis is a widely used technique to examine the electrochemical active surface area (ECSA) of proton exchange membrane fuel cell (PEMFC) electrodes [1]. During CVs, currents associated to adsorption limited electron-transfer reactions on the catalyst surfaces are measured as a response to potential scans. The ECSA is then

determined either from the electrical charges transferred during the under-potential deposition of hydrogen (H_{UPD}) or from the charges associated to the oxidation of adsorbed carbon monoxide (CO) referred to as CO-stripping [2, 3]. The former is conducted in an atmosphere of hydrogen (H₂) and nitrogen (N₂) in the counter and working electrode (WE), respectively, while the latter requires a CO adlayer adsorbed on the electrocatalyst in the WE prior to the actual CV. For alloyed electrocatalysts and/or supports, CO-stripping or a combination of both methods is preferable, as the charge transfer reactions and therefore CV profiles often are affected by the added alloy elements [4–6]. In contrast, for pure polycrystalline platinum supported on carbon (Pt/C), ECSA determination via H_{UPD} often is considered sufficient as it eliminates the provision of an additional CO/N₂ gas mixture required for CO-stripping. For Pt/C electrocatalysts, the basic reactions during H_{UPD} are the adsorption/desorption of atomic hydrogen (H) and the oxidation/reduction of platinum (Pt) and its oxide (PtOx), respectively, as shown in Fig. 1a.

From these CV profiles, the ECSA is determined via integration of the H-adsorption and/or H-desorption currents

✉ S. Prass
sebastian.prass@ise.fraunhofer.de

¹ Fraunhofer Institute for Solar Energy Systems ISE, Heidenhofstr. 2, 79114 Freiburg, Germany

² Hawaii Natural Energy Institute, University of Hawaii, Manoa, 1680 East-West Road, POST 109, Honolulu, HI 96822, USA

³ Institute of Engineering Thermodynamics, German Aerospace Center, Pfaffenwaldring 38-40, 70569 Stuttgart, Germany

⁴ Institute of Building Energetics, Thermal Engineering and Energy Storage (IGTE), University of Stuttgart, Pfaffenwaldring 31, 70569 Stuttgart, Germany

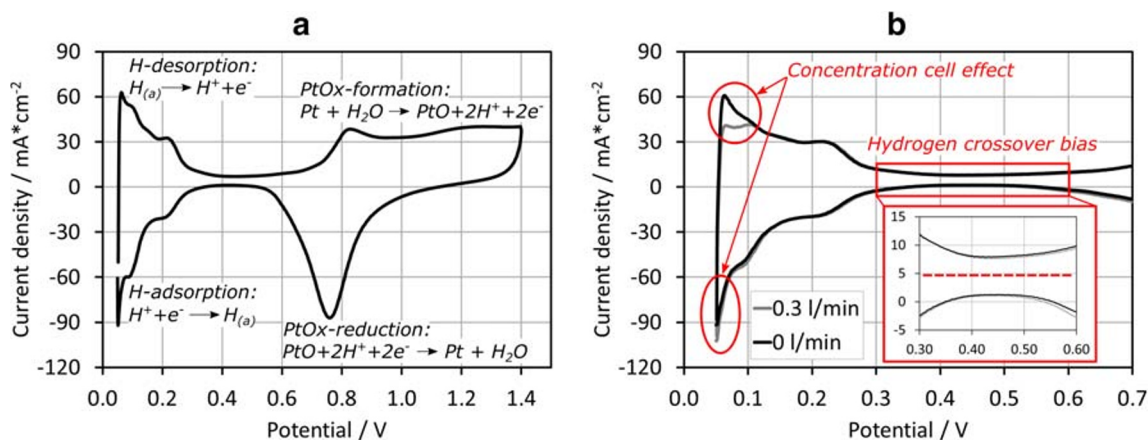


Fig. 1 Typical CV profile of a Pt/C electrocatalyst (a) and its artifacts such as the “concentration cell effect” and “hydrogen crossover bias” (here: ~ 5 mA/cm² as shown in the inset) (b). The formation and reduction of PtOx is presented figuratively by the reactions including

(between ~ 0.08 and 0.4 V) by subtraction of the charge transfer associated to the double-layer charging (typically between 0.3 and 0.6 V) [3]. In contrast, the currents associated to formation (anodic transient, above 0.7 V) and reduction of PtOx (cathodic transient, between 0.5 and 1 V) are of interest, if the reversibility of structural and chemical changes in the catalyst [6–11] or support surfaces [12] or the presence of impurities on these surfaces [13, 14] are to be examined. These oxide formation and reduction processes are more complex as H-adsorption/desorption, as they often include the ad- or desorption of water, subsequent multi-step electron transfer reactions via hydroxide formation, and different oxidation states of the catalyst depending on the potential range [15–19].

As several research groups have already reported, artifacts during CV measurements distort the CV profiles and thereby affect extracted information such as the ECSA [20, 21]. One of these artifacts is the “concentration cell effect” shown in Fig. 1b, caused by the superposition of molecular H₂ evolution current, which depends on the partial H₂ pressure in the WE, and currents from H-adsorption/desorption [22]. With higher N₂ flowrates, molecular H₂ is purged from the WE, the partial H₂ pressure decreases, and more H₂ evolves in the WE showing as increased negative currents in CV profiles below 0.1 V. Another artifact arises due to molecular H₂ crossing over through the membrane to the WE (H_{2X}), where it readily oxidizes at potentials above 0.1 V, generating a bias current that shifts the center of the CV profile away from the x -axis (e.g., 5 mA/cm² in Fig. 1b).

In addition to these two well-known phenomena, we observed another artifact during CV analysis of low- and ultra-low-loaded electrodes during the cathodic scan at potentials between 0.6 and 0.8 V, which is shown in Fig. 2. The artifact is visible as a positive oxidation peak where the negative PtOx reduction peak would be expected, which is more pronounced for lower Pt loadings in the electrode (Fig. 2b). Understanding

PtO; however, further oxide species such as PtOH or PtO₂ are present depending on the upper potential sweep limit and catalyst material. Scan rate: 100 mV/s; N₂ purge: 0 and 0.3 l/min; $p_{\text{an}}/p_{\text{ca}}$: $50/50$ mbar

this type of artifact is particularly important as low-loaded electrodes (loadings ≤ 100 $\mu\text{g}/\text{cm}^2$ of an electrocatalyst) are increasingly employed especially in the anode electrode of automotive catalyst-coated membranes (CCMs) [23]. Platinum loadings of 50 $\mu\text{g}/\text{cm}^2$ are already often considered state-of-the-art, with even lower (ultra-low) loadings forecasted for the near future. Although the majority of studies in literature focuses on the cathode electrode including higher catalyst loadings and its decay during accelerated stress tests (ASTs), the anode electrode is of interest especially when investigating the effect of startup/shutdown cycles [24] or impurities [25, 26] on the anode compartment, or the cell reversal tolerance upon freeze start-ups and successional reversal effects [27, 28]. Therefore, thorough understanding of CVs of low- and ultra-low-loaded electrodes is of great interest.

In literature, few comparable oxidation peaks during the reverse (cathodic) scan of CVs have been reported. Tahmasebi et al. [29] investigated electrocatalytic reactions occurring on a Pt wire acting in an all-glass electrochemical cell under atmospheres saturated with N₂, oxygen (O₂), or H₂ and found this oxidation peak during the cathodic scan, once the setup and electrode was saturated with H₂. They associated this peak to an “increased catalytic activity” towards H₂ oxidation reaction (HOR), which indicates the necessity of H₂ to be present for the artifact to occur. For PEMFCs operating with alcohols such as methanol (MeOH), Zhao et al. [30] discussed a comparable oxidation peak during the cathodic scan regularly observed for MeOH-PEMFCs [31–33], as there exist two theories on its origin. The older theory associates this peak to the oxidation of CO forming inevitably during the reaction of MeOH on electrocatalysts, while the newer theory demonstrates that the peak is caused by MeOH reacting on freshly formed sites after the reduction of the catalyst oxides during the cathodic CV transient. For PEMFCs operated with H₂ and O₂/air (H₂ and N₂ during CVs), to the best of our

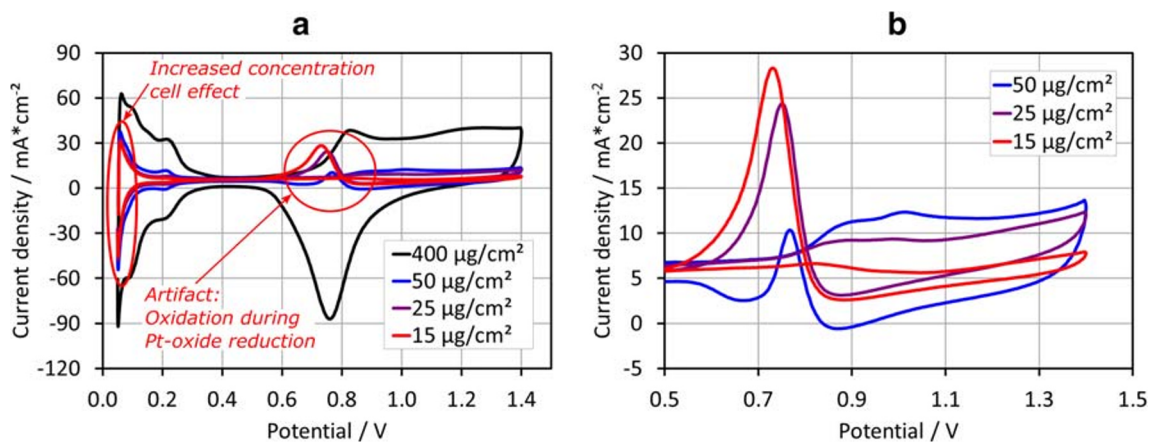
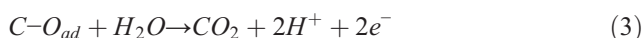
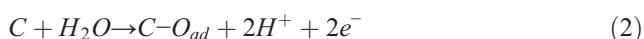
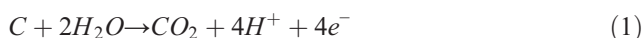


Fig. 2 CVs of a high-loaded electrode ($400 \mu\text{g}/\text{cm}^2$) versus CVs of low and ultra-low-loaded electrodes (50 , 25 , and $15 \mu\text{g}/\text{cm}^2$) in comparison (**a**). For the low-loaded electrodes, the concentration cell effect appears increased in comparison to currents associated to H-adsorption and H-

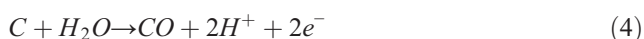
desorption, and additionally the artifact peak shows where the PtOx reduction is expected during the cathodic scan (**b**). Scan rate: $100 \text{ mV}/\text{s}$; N_2 purge: $0 \text{ l}/\text{min}$; $p_{\text{an}}/p_{\text{ca}}$: $50/50 \text{ mbar}$

knowledge, this oxidation peak during the cathodic transient has not yet been reported in literature.

The intuitive assumption that this artifact could originate from the oxidation of carbon surface species such as carbon oxides formed on the support of catalyst particles, is comprehensible. Carbon surface oxides, which are regarded as reaction intermediates during the carbon corrosion process, can form at elevated potentials depending on the type and surface defect density of the carbon support and the presence of catalyst material [34–39]. Maass et al. [37] characterized five distinct carbon corrosion processes in different potential regimes, of which three processes could be linked to the artifact described in our study as they eventually occur at elevated potentials during potentiodynamic measurements. At potentials above 0.207 V vs. RHE, carbon oxidation to carbon dioxide (CO_2) generally takes place either directly according to reaction (1) or indirectly with carbon surface oxides (O_{ad}) forming as intermediate species according to reactions (2) and (3), respectively.



Moreover, carbon monoxide (CO) can form at potentials above 0.518 V vs. RHE according to reaction (4).



Luckily the reaction kinetics of carbon oxidation are sluggish at potentials below ~ 0.9 – 1 V enabling the use of carbon as catalyst support material for PEMFCs [40]. At higher potentials and especially in presence of Pt, the reaction kinetics significantly increase, which results in significant corrosion rates and the loss of carbon support material [34, 38]. If O_{ad}

or CO species formed via reactions (2) and (4) and remained stable long enough even at elevated potentials during potentiodynamic cycling, these species could oxidize with hydroxyl groups on Pt surfaces stemming from the reduction of PtOx according to reaction (5), which could result in the artifact peak in the potential window of ~ 0.6 – 0.8 V .



Carbon oxidation is expected to proceed to a certain degree during elevated potential cycling of Pt/C electrodes. Consequently, some carbon oxide species could form and be available for oxidation during the reduction of PtOx causing the artifact peak. Another alternative explanation could be linked to the study by Yamashita et al. [41]. The authors investigated carbon corrosion mechanisms during shut-down and start-up procedures while varying the atmosphere in the WE and formulated three different carbon corrosion mechanisms correlated to PtOx reduction. These mechanisms are all based on shortages of either gaseous H_2 or protons and electrons required for the chemical reaction or reduction of PtOx and which are inherently generated by the oxidation of the carbon support. With respect to the artifact, some of these generated protons and electrons could be transferred towards the CE compartment instead of reducing PtOx, resulting in the artifact peak. However, based on the experiments conducted in our study, these alternative explanations including carbon corrosion processes seem unlikely as compared to the accumulation and spontaneous HOR of crossover hydrogen outlined in the following section.

In this paper, we present the results from the investigations into the artifact visible during CV analysis of low-loaded PEMFC Pt/C electrodes. CV as well as linear sweep voltammetry (LSV) measurements have been conducted on electrodes with different Pt/C loadings while varying the measurement

parameters such as the N_2 purge rate and gas pressures in anode and cathode (p_{an}/p_{ca}) as well as the CV settings such as the upper potential limit and scan rate. These variations aim on elucidating the correlation between cell environment and artifact occurrence and magnitude to clarify its origin.

Experimental

For this study, all CV and LSV measurements were conducted in a balticFuelCells GmbH qCf *Liquid Cooling high amp* differential cell at 80 °C cell temperature in a fuel cell test bench designed and built in-house. For each measurement, the cell was purged with fully humidified (100% relative humidity) H_2 (quality 5.0, Linde AG) and N_2 (quality 6.0, Air Liquide) prior to the CV or LSV. Unless noted otherwise, the N_2 purge of the WE was switched off 5 s prior to starting the CV measurement, allowing stagnant N_2 in the compartment. The CE was purged with 0.3 l/min H_2 . Also, for most CV measurements, the gas pressure in both electrodes was set to 50 mbar_g during the CV to avoid intrusion of ambient air. CV analysis was performed by cycling the potential between 0.05 and the respective upper potential limit vs. reversible hydrogen electrode (RHE) at varying scan rates for 5 full cycles. Any variations in measurement parameters or CV settings are given in the figure captions and corresponding text.

The measurements were conducted on three different CCMs (provided by Greenerity GmbH) with equal membranes and cathode catalyst layers (CLs), but with different low loadings on the anode. In all CCMs, the cathode contained the same 400 $\mu\text{g}/\text{cm}^2$ of Pt on highly graphitized carbon, while the anode contained either 50, 25, or 15 $\mu\text{g}/\text{cm}^2$ of Pt on high surface area carbon. All electrodes were fabricated in a similar manner, but the different loadings were achieved by varying the thicknesses of the electrodes. Freudenberg H23 C9 was employed as gas diffusion layer (GDL) material in both anode and cathode compartments. All CV measurements on low-loaded electrodes were carried out with the anode as working electrode (WE).

Results and Discussion

As can be seen in Fig. 2b, the artifact was visible for all low-loaded electrodes (50, 25, and 15 $\mu\text{g}/\text{cm}^2$). However, it appeared the strongest for the electrode with the lowest loading of 15 $\mu\text{g}/\text{cm}^2$. Therefore, in order to enhance the visibility of effects due to parameter variation, we present predominantly the results of CV analysis of this electrode in the following sections.

Most studies in literature employ CV scan rates between 1 and 100 mV/s [20, 21, 26, 42, 43]. At higher scan rates, current magnitudes arising from electrochemical surface

processes generally increase. Simultaneously, depending on the reaction rate of the process, the potentials at which these magnitudes are reached can shift while transferred charges associated to a process can decrease if the process is not given sufficient time to terminate. However, for ultra-low-loaded and thin electrodes, relatively high scan rates were found to enhance the distinction of electrochemical processes from CV profiles for subsequent analysis. Additionally, higher scan rates allow for shorter dwell times of the WE at potentials > 0.85 V avoiding unnecessary carbon corrosion of the catalyst support. Therefore, to investigate the artifact, we conducted and analyzed CV profiles predominantly taken at relatively high scan rates of 100 and 400 mV/s. However, the artifact peak was also observed for lower CV scan rates of 20 mV/s as can be seen in Fig. 4a.

N_2 Purge and Upper Potential Limit Variations

Figure 3 presents CV profiles taken at 400 mV/s of the lowest electrode loading (15 $\mu\text{g}/\text{cm}^2$) with varying upper potential limits (0.7 to 1.4 V in 0.1 V steps), when the N_2 purge was switched on and off.

In Fig. 3a and b, the features of the anodic and cathodic transients in the potential range from 0.1 to 0.3 V correspond to desorption and adsorption of H_{UPD} , whereas the relatively large currents below 0.1 V correspond to H_2 evolution at the WE. With N_2 purge being switched off, H_2 evolves and accumulates in the WE resulting in the oxidation currents at the onset of the anodic transient. At potentials of 0.8–1.4 V in the anodic transient, Pt oxidizes to form PtOx, which is reduced at potentials of 0.5–1.0 V in the cathodic transient mainly visible in the CV profiles taken with N_2 purge being switched on. In contrast, with the N_2 purge being switched off, the artifact peak occurred as shown in Fig. 3b at potentials below 0.8 V including a relatively steep incline and drop in current partly overlapping the PtOx reduction potential, as well as a gradient decline in current in the double-layer region at potentials of 0.3–0.6 V. All shown CV profiles include a positive bias due to crossover hydrogen (H_{2X}), which should be similar for all CV profiles as measurements were typically conducted successively on one CCM sample. Although CV profiles generally can be corrected via subtraction of the bias, the artifact oxidation peak would not allow for clear evaluation of the bias magnitude according to the inset of Fig. 1b. Therefore, all CV profiles reported here are not centered on the x -axis.

Evidently, the artifact peak only becomes visible when the N_2 purge is switched off. Furthermore, the current magnitude of the artifact increases while the peak potential decreases, when the upper CV potential limit reaches further into PtOx formation potentials. Firstly, this observation hints towards a gaseous species required for the artifact to occur, as such a species could be purged out of the WE with N_2 . Presumably, carbon oxide species residing on the surface of the carbon

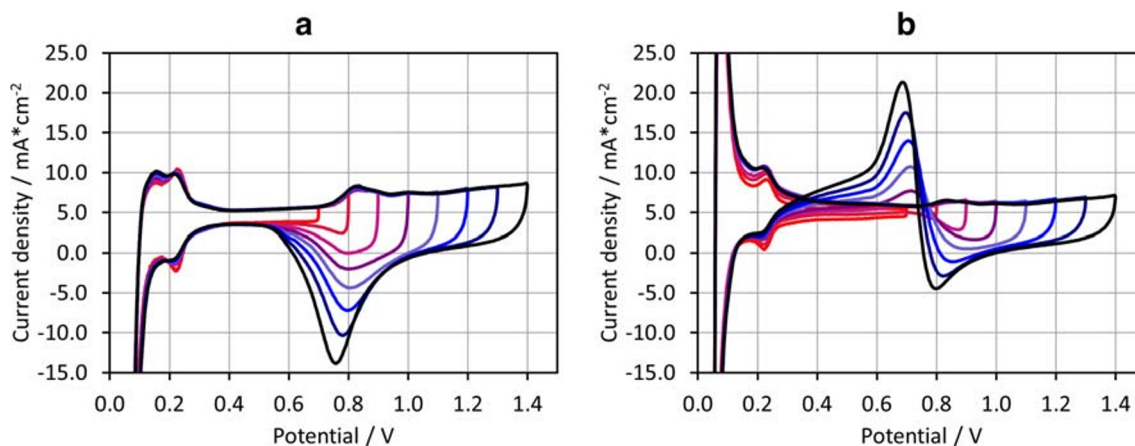


Fig. 3 Variation of the upper potential limit with N₂ purge on the WE switched on (a) and off (b). Electrode: 15 μg/cm²; scan rate: 400 mV/s; P_{an}/P_{ca}: 50/50 mbar

support near Pt particles would not be affected by the N₂ purge, thus eliminating the theory including such carbon surface oxides. Secondly, the growth in artifact magnitude with increasing CV upper potential limit indicates a dependency of the artifact either on the PtOx layer and/or on the dwell time the WE remains at specific potentials, during which a species could form. Though carbon corrosion takes place and eventually produces carbon dioxide, the formation of gaseous trace carbon monoxide seems unlikely considering its instability at elevated potentials especially in the presence of Pt.

Scan Rate Variations

One way to investigate electrochemical processes and to distinguish between Faradaic and surface electrochemical reactions is to conduct CVs at different potential scan rates, since changes in current magnitudes or transferred charges with scan rate variations can offer valuable information about the origin of an observed process. For this purpose, Fig. 4a presents CV profiles of the 15 μg/cm² electrode obtained at

different potential scan rates (20 mV/s and 100 to 800 mV/s in 100 mV/s steps), without N₂ purge of the WE.

Again, in Fig. 4a, both desorption and adsorption of H_{UPD} are visible between potentials of 0.1 and 0.3 V, while the large currents below 0.1 V correspond to H₂ evolution at the WE. At potentials of 0.8–1.4 V, PtOx formation occurs, which shows as increasing positive currents in CV profiles conducted at scan rates > 300 mV/s. At lower scan rates, the currents in the potential window decrease due to the decrease in H₂X bias as a result of PtOx formation, which will be explained in more detail in the following section. During the cathodic CV transient, PtOx reduction proceeds at potentials of about 0.7 to 1.1 V. Typically, the reduction would continue to even lower potentials of about 0.6 [29], but the artifact appears as a positive oxidation peak overlapping the reduction current. With higher scan rates, the artifact starts at lower potentials (E_{Redr}), inset of Fig. 4b) and reaches lower peak currents (i_{Peak}) at lower peak potentials (E_{Peakr}), which coheres with the decrease in PtOx reduction currents reached at lower E_{Redr} potentials. Furthermore, the potential at which the artifact finishes (E_{Int}) decreases with higher scan rates. However, for few CV

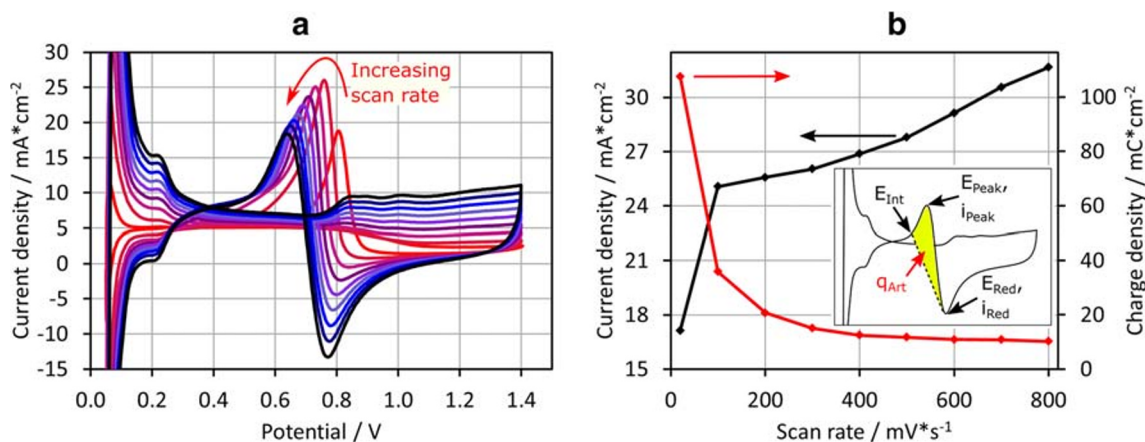


Fig. 4 Scan rate variation (20, 100–800 mV/s in 100 mV/s steps) without N₂ purge on the WE (a) and peak current of the artifact as well as the transferred charge from areas integrated as shown in the inset (b). Electrode: 15 μg/cm²; P_{an}/P_{ca}: 50/50 mbar

profiles taken at relatively low scan rates, the latter value (E_{Int}) is difficult to extract and, hence, the potential was arbitrarily selected as the potential where the steep decline in current after the artifact peak ends.

Typically, in case of only oxidation or reduction processes eventually overlapping (such as adsorption/desorption of H_{UPD} and double-layer charging), the change in current magnitude would be of interest when conducting CV scan rate variations. Unfortunately, in case of the artifact, the artifact oxidation current overlaps partially with the PtOx reduction current, which significantly affects the magnitude i_{Peak} . However, as a substitute and to predominantly examine the current associated with the artifact, the difference in currents $i_{\text{Art}} (= i_{\text{Peak}} - i_{\text{Red}})$ between the onset and completion was extracted instead and plotted in Fig. 4b along with the charge q_{Art} . For q_{Art} , the integration area as shown in the inset of Fig. 4b is based on the assumption that the lowest PtOx reduction current (i_{Red} , E_{Red}) marks the starting point of the artifact, while the end point is resembled by the change in inclination in the declining branch (E_{Int}). This area is selected arbitrarily and likely includes errors arising from the overlap with the PtOx reduction currents or the difficulty to assess the true boundaries of the artifact. However, for most observed artifact peaks, the boundaries distinctly marked an area of positive oxidation currents especially for the electrode loadings of 50 and 25 $\mu\text{g}/\text{cm}^2$ as can be seen in Fig. 6. Table 1 lists the respective values for i_{Art} , E_{Peak} , E_{Red} , and E_{Int} as well as the transferred charges q_{Art} of the CV profiles in Fig. 4a.

Generally, if the current associated to a process increases proportionally with the increase in scan rate, while simultaneously the transferred charges integrated between potential limits remain approximately constant, the process can be associated to either a non-Faradaic or a Faradaic process controlled by surface electrochemical processes as e.g. double-layer charging or H-adsorption. For example, if all Pt sites are occupied by atomic hydrogen, the doubling in scan rate will result in twice the current magnitude in the potential range of 0.1–0.3 V, while integration would result in an almost constant charge transfer as H-adsorption and double-layer charging are

relatively fast processes [29]. Vice versa, a disproportional change in current and significant differences in transferred charges would hint towards a Faradaic process, which is controlled or dominated by the diffusion of reactants and/or products. From Fig. 4b, the artifact current i_{Art} shows a rather disproportional increase, while the transferred charges q_{Art} decrease exponentially. Therefore, both the unsteady increase in artifact current i_{Art} and exponential decay of the charge q_{Art} with increasing scan rate rather support the definition of Faradaic reactions. The large offset of i_{Art} for the scan rate of 20 mV/s presumably is a result of the interplay between PtOx reduction and artifact oxidation processes at different reaction rates, which emerges at relatively low scan rates.

To confirm whether PtOx is responsible for the decrease in $\text{H}_{2\text{X}}$ -related bias at scan rates < 300 mV/s in Fig. 4a, we conducted LSVs with all three low-loaded electrodes in comparison to the high-loaded electrode of 400 $\mu\text{g}/\text{cm}^2$ at a scan rate of 1 mV/s as shown in Fig. 5.

The response of the low-loaded electrodes upon the potential increase is a direct decrease in the $\text{H}_{2\text{X}}$ -related current at potentials > 0.5 V and a flattening of the current towards the upper potential limit of 1 V. In comparison, the current of the 400 $\mu\text{g}/\text{cm}^2$ electrode first increases and then drops after potentials above 0.7 V, but it does not level out at about 1 V. Higher potentials were avoided during these LSV measurements, as the scan rate of 1 mV/s would be inevitably accompanied with unnecessary dwell times at potentials critical for corrosion of the carbon support [10, 36]. While some studies point towards a complete suppression of HOR on PtOx [44–46], a newer study presents an improved HOR and H_2 evolution reaction (HER) activity of synthesized Pt-(PtOx)-Nitrogen doped hybrid catalysts [47]. In a study by Iden et al. [48], the authors correlate the decrease in $\text{H}_{2\text{X}}$ limiting current density to the increase in mass transfer losses due to the loss in effective ECSA, when Pt sites are blocked by surface oxides at elevated potentials. Whether PtOx affects HOR/HER depends on the electronic and electrochemical properties of the Pt particles, interactions with possible alloying components in and on the carbon support, the uniformity of the PtOx coverage, which

Table 1 Currents associated to the artifact (i_{Art}) and potentials of its onset (E_{Red}), peak (E_{Peak}), and completion (E_{Int}) as well as the transferred charge q_{Art} integrated from the yellow area from Fig. 4b per scan rate s

s (mV/s)	q_{Art} (mC cm^{-2})	i_{Art} (mA cm^{-2})	E_{Peak} (V)	E_{Red} (V)	E_{Int} (V)
20	107.5	17.1	0.806	0.934	0.752
100	35.9	25.1	0.758	0.863	0.673
200	20.7	25.6	0.730	0.838	0.635
300	15.0	26.0	0.709	0.811	0.611
400	12.5	26.9	0.689	0.798	0.594
500	11.7	27.8	0.673	0.785	0.561
600	10.9	29.1	0.660	0.779	0.550
700	10.8	30.6	0.649	0.775	0.528
800	10.2	31.7	0.637	0.771	0.520

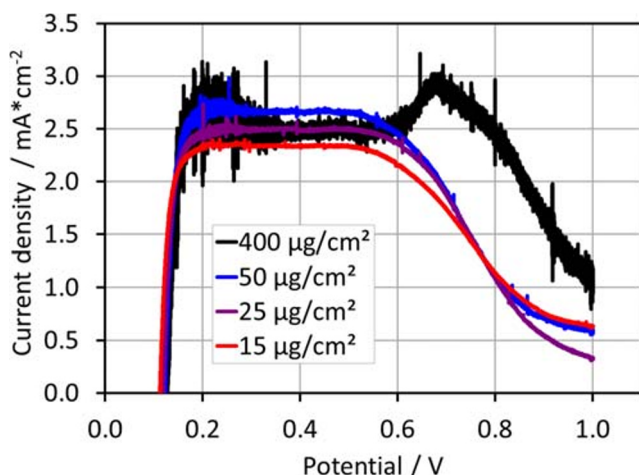


Fig. 5 LSV measurements corrected for IR (resistance from slope between 0.3 and 0.5 V). Scan rate: 1 mV/s; P_{an}/P_{ca} : 50/50 mbar; flow rate f_{an}/f_{ca} : 1/1.2 l/min

itself depends on the type and orientation of the underlying Pt particle facets [49], respectively, and if nothing else, on the medium (acidic or alkaline environment). Either way, for the LSV profiles shown in Fig. 5, it is safe to assume that the drop in current at potentials >0.6 V can be associated with the effect of PtOx on HOR. Similarly, the decrease in current at potentials >0.8 at scan rates <300 mV/s in the CV profiles shown in Fig. 4 can also be linked to the decreasing H_{2X} bias overlapping the current associated to Pt oxidation. Since molecular H_2 continues to cross over through the PEM also when PtOx suppresses the HOR, the H_{2X} must accumulate in the WE. This is consistent with the observation that the artifact is suppressed once the N_2 flow is switched on and H_{2X} is purged out of the WE.

Gas Pressure Variations

To test whether crossover hydrogen (H_{2X}) is the species responsible for the artifact, CV measurements at varying gas pressures in the CE and WE (p_{CE}/p_{WE}) were conducted. Higher gas pressures in the CE as compared to the WE would lead to higher crossover rates and, therefore, are expected to affect the magnitude or transferred charge of the artifact. Figure 6 shows the CVs conducted at gas pressure variations between 50 and 600 mbar_g in CE and WE for all three low-loaded electrodes (50, 25, and 15 $\mu\text{g}/\text{cm}^2$).

Again, the CV profiles include currents associated to H-adsorption and H-desorption (between 0.1 and 0.3 V) as well as Pt oxidation (during anodic scan, between 0.8 and 1.4 V) and PtOx reduction (during cathodic scan, between 0.5 and 1 V). Also, for lower electrode loadings, the artifact peaks appear increased relative to currents associated to H_{UPD} or PtOx formation and reduction. Moreover, with higher pressures in the CE (600/50, 400/50, and 200/50), the CV profiles

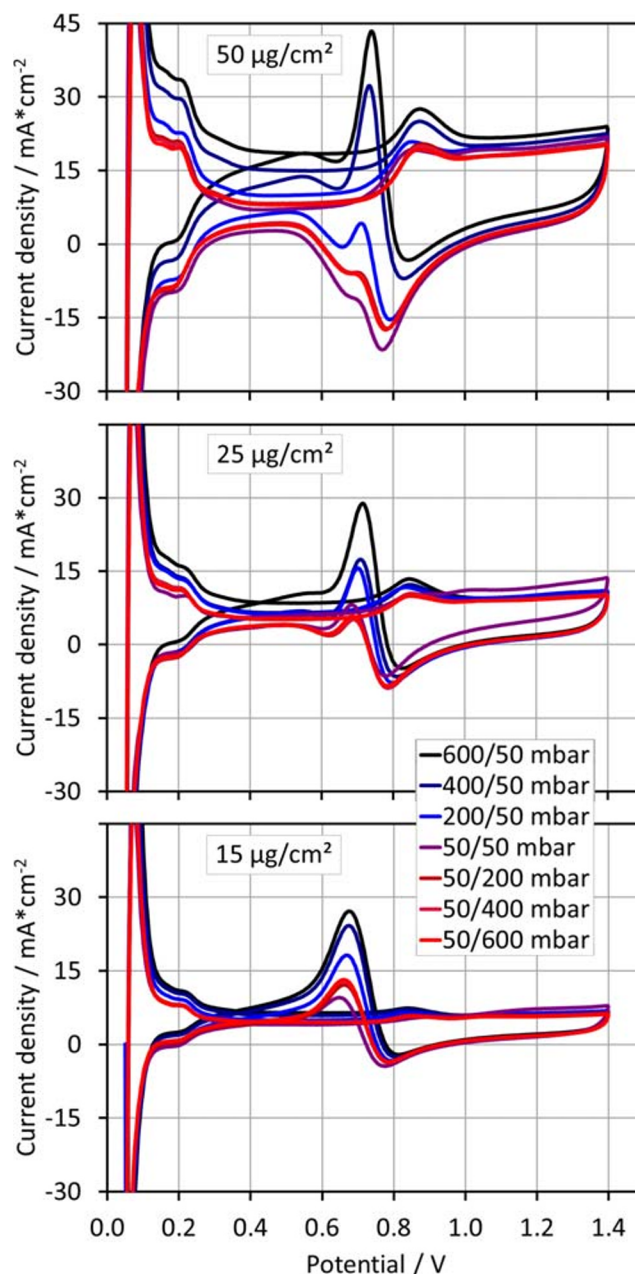


Fig. 6 Variation of gas pressures between 50 and 600 mbar_g on anode/cathode for the 50, 25, and 15 mg/cm^2 electrodes. Scan rate: 400 mV/s

include an enhanced bias upwards from the x -axis as a result of an increased H_{2X} while simultaneously the artifact peaks appear enhanced for all electrode loadings. To facilitate this observation, Fig. 7 shows the artifact currents I_{Art} as well as the charges transferred q_{Art} integrated again as shown in the inset of Fig. 4b.

As can be seen, I_{Art} (solid line) and q_{Art} (dashed line) significantly increase with higher gas H_2 pressures in the CE (left hand side from p_{CE}/p_{WE} 50/50), indicating the correlation between the artifact and H_{2X} . Interestingly, slight increases in I_{Art} and q_{Art} are apparent also at higher pressures in the WE

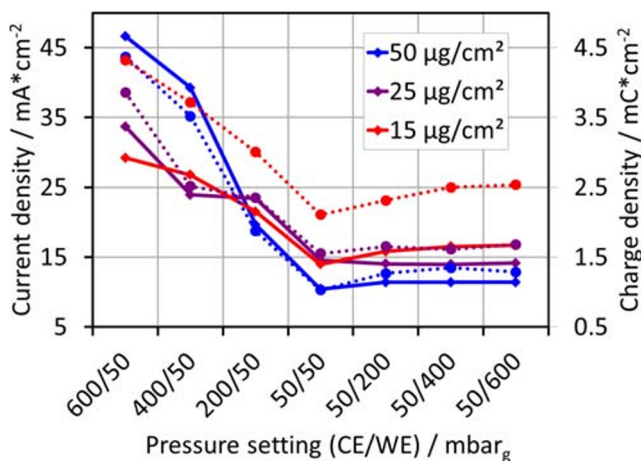


Fig. 7 Peak current (solid line) and transferred charges (dashed line) integrated as shown in the inset of Fig. 4b of all three low-loaded electrodes from CVs in Fig. 6

(right hand side from $p_{\text{CE}}/p_{\text{WE}}$ 50/50), which could be due to an increased activity of $\text{H}_{2\text{X}}$ at higher gas pressures in the WE and therefore increased HOR rates. Again, the values used for Fig. 7 are listed in Table 2.

From the pressure variations during the CV measurements, it is evident that with higher H_2 pressures in the CE, more H_2 crosses through the membrane and the larger the artifact peak

occurs (at a given Pt loading), if the N_2 purge of the WE is switched off. Based on the findings, the artifact

- Most likely is a Faradaic process limited by the presence of a species
- Only appears if N_2 purge is switched off such that a gaseous species can accumulate
- Appears for electrodes which fully passivate towards $\text{H}_{2\text{X}}$ -related currents at oxide formation potentials
- Increases with higher gas pressures in the CE, i.e., higher $\text{H}_{2\text{X}}$ rates

Consequently, we hypothesize that the artifact originates from crossover hydrogen ($\text{H}_{2\text{X}}$), which collects at the WE as soon as the electrode is passivated due to PtOx coverage. With the reduction of the oxide during the cathodic scan, active metallic catalyst sites are freed and made available for the spontaneous HOR of the accumulated $\text{H}_{2\text{X}}$ as shown schematically in Fig. 8.

This process occurs in three main steps; (1) PtOx formation and coverage of the Pt sites takes place in the anodic scan, while $\text{H}_{2\text{X}}$ accumulates in the catalyst layer simultaneously; (2) a full PtOx coverage is obtained with $\text{H}_{2\text{X}}$ accumulated in the pore space of the catalyst layer; (3) HOR of the accumulated $\text{H}_{2\text{X}}$ commences as the potential drops during the

Table 2 Currents associated to the artifact (i_{Art}) and potentials of its onset (E_{Red}), peak (E_{Peak}), and completion (E_{Int}) as well as the transferred charge q_{Art} per pressure setting on anode/cathode

p (CE/WE) (mbar)	q_{Art} (mC cm^{-2})	i_{Art} (mA cm^{-2})	E_{Peak} (V)	E_{Red} (V)	E_{Int} (V)
50 $\mu\text{g}/\text{cm}^2$					
600/50	4.4	46.7	0.740	0.842	0.642
400/50	3.5	39.3	0.734	0.829	0.642
200/50	1.9	19.6	0.710	0.792	0.665
50/50	1.0	10.4	0.706	0.771	0.669
50/200	1.3	11.4	0.706	0.784	0.665
50/400	1.3	11.4	0.706	0.781	0.665
50/600	1.3	11.4	0.706	0.781	0.665
25 $\mu\text{g}/\text{cm}^2$					
600/50	3.9	33.7	0.713	0.618	0.822
400/50	2.5	23.9	0.710	0.611	0.809
200/50	2.4	23.4	0.703	0.614	0.798
50/50	1.6	14.5	0.686	0.604	0.778
50/200	1.7	14.1	0.689	0.622	0.784
50/400	1.6	14.0	0.689	0.622	0.784
50/600	1.7	14.2	0.686	0.611	0.784
15 $\mu\text{g}/\text{cm}^2$					
600/50	4.3	29.2	0.676	0.557	0.815
400/50	3.7	26.8	0.676	0.560	0.805
200/50	3.0	21.5	0.669	0.567	0.795
50/50	2.1	14.0	0.649	0.564	0.774
50/200	2.3	15.8	0.662	0.564	0.788
50/400	2.5	16.5	0.659	0.567	0.784
50/600	2.5	16.7	0.659	0.570	0.788

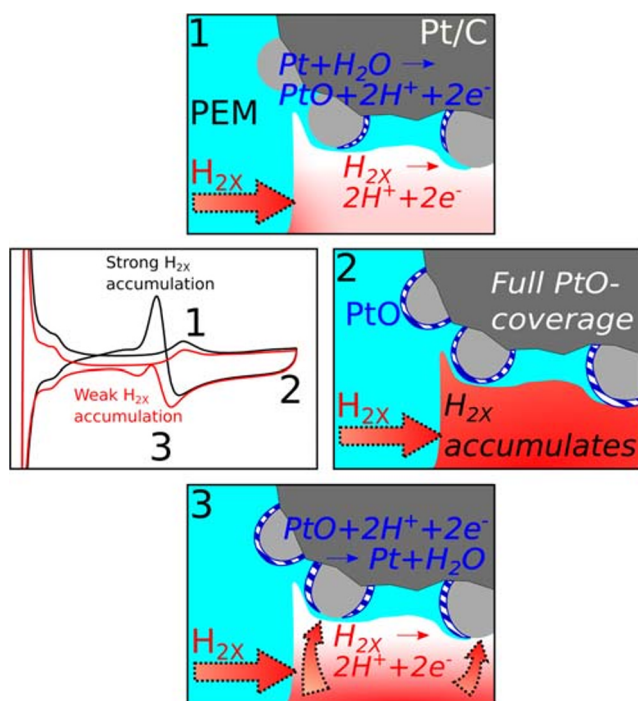


Fig. 8 Schematic of H_{2X} accumulation during PtOx formation and spontaneous HOR during PtOx reduction

cathodic scan and PtOx reduction frees metallic catalyst sites. The magnitude of the HOR peak depends on the ratio of the amount of accumulated H_{2X} in the pore spaces and the product of PtOx reduction and HOR currents. If PtOx reduction currents dominate as it is observed for higher catalyst loadings, the HOR peak appears smaller with all other conditions unchanged. Also, H_{2X} accumulations are weakened if an N_2 flow purges hydrogen out of the pore spaces in the WE. In contrary, the HOR peak increases for stronger H_{2X} accumulations caused by higher H_{2X} diffusion rates through the PEM, as it is the case for elevated gas pressures in the CE and as it is expected for lower PEM thicknesses or PEM ionomers allowing for increased hydrogen gas crossover. The upper potential limit and scan rate of the CV show mixed effects, as these parameters both determine the time for the processes of H_{2X} to accumulate and PtOx to form and, hence, the net effect depends on the relative rates of the respective processes.

Consequences for CV Analysis

Depending on the electrode material analyzed, the artifact can emerge during CV analysis of low-loaded electrodes when the N_2 purge is switched off during the measurement and the upper CV potential limit reaches into oxide formation potentials. If these requirements are met and the artifact appears, it eventually interferes with ECSA determination from H-adsorption due to difficulties in determining the starting point of H-adsorption between potentials of 0.3 and 0.6 V in the cathodic transient. Moreover, a comparison between the charges transferred during

Pt oxide formation and reduction loses significance, as PtOx reduction is overlapped by the artifact. When selecting an upper potential limit below oxide formation potentials and/or employing N_2 purge rates of the WE as it is typically done for CV analysis, the artifact will not appear. However, the existence of this artifact has also consequences for the operation of low-loaded cathode CCMs. In operation conditions where PtOx is formed, we have to assume that H_{2X} can accumulate on the cathode side as it is not active enough for HOR. This can lead to safety concerns or at least to reaction heat evolution when PtOx reduction takes place with possibly enhanced degradation. It is certainly an effect to be considered carefully in operation of low-loaded CCMs.

Conclusion

In this study, we investigate an artifact peak overlapping the PtOx reduction peak measured in the cathodic transient of cyclic voltammetry analysis of ultra-low-loaded catalyst layers through a parametric analysis. Considering findings by Tahmasebi et al. [29] and Zhao et al. [30] with respect to comparable oxidation peaks, we conclude that this peak is caused by spontaneous HOR of previously accumulated crossover hydrogen (H_{2X}). Two requirements must be fulfilled for this feature to be measured. First, this feature is expected to occur predominantly during CV analysis of low and ultra-low-loaded electrodes composed of catalyst material whose oxide is completely inactive towards HOR. Second, the CV measurements must be carried out without N_2 purge of the WE. For higher loaded electrodes, the artifact is not observed as Pt or alloys including Pt are either not fully covered by an oxide layer upon reversal of the transition from anodic to cathodic transient, and/or the currents associated with the oxide reduction are much larger than the spontaneous HOR of accumulated H_{2X} . If the requirements are met and artifact appears, it can interfere with ECSA determination from H-adsorption currents and with analysis of currents associated to Pt oxide formation and reduction. With the expected cuts in noble metal loadings of catalyst-coated membranes for automotive applications, this artifact might be observed more often in the future.

Acknowledgements Open Access funding enabled and organized by Projekt DEAL.

Funding This work was supported by the German Federal Ministry for Economy and Energy within the project HAIMa, contract No. 03ET6098A.

Compliance with Ethical Standards

Conflict of Interest The authors declare that they have no conflict of interest.

Open Access This article is licensed under a Creative Commons Attribution 4.0 International License, which permits use, sharing, adaptation, distribution and reproduction in any medium or format, as long as you give appropriate credit to the original author(s) and the source, provide a link to the Creative Commons licence, and indicate if changes were made. The images or other third party material in this article are included in the article's Creative Commons licence, unless indicated otherwise in a credit line to the material. If material is not included in the article's Creative Commons licence and your intended use is not permitted by statutory regulation or exceeds the permitted use, you will need to obtain permission directly from the copyright holder. To view a copy of this licence, visit <http://creativecommons.org/licenses/by/4.0/>.

References

- W. Vielstich, A. Lamm, H.A. Gasteiger, *Handbook of Fuel Cells - Fundamentals, Technology and Applications*, vol. 3, Part 1; John Wiley & Sons, Inc. (2003)
- G. Jerkiewicz, Electrochemical hydrogen adsorption and absorption. Part 1: Under-potential deposition of hydrogen. *Electrocatalysis* **1**(4), 179–199 (2010). <https://doi.org/10.1007/s12678-010-0022-1>
- M. Lukaszewski, M. Soszko, A. Czerwiński, Electrochemical methods of real surface area determination of noble metal electrodes - an overview. *Int. J. Electrochem. Sci* **11**(6), 4442–4469 (2016). <https://doi.org/10.20964/2016.06.71>
- S. Rudi, C. Cui, L. Gan, P. Strasser, Comparative study of the electrocatalytically active surface areas (ECSAs) of Pt alloy nanoparticles evaluated by Hupd and CO-stripping voltammetry. *Electrocatalysis* **5**(4), 408–418 (2014). <https://doi.org/10.1007/s12678-014-0205-2>
- I.C. Halalay, S. Swathirajan, B. Merzougui, M.P. Balogh, G.C. Garabedian, M.K. Carpenter, Anode materials for mitigating hydrogen starvation effects in PEM fuel cells. *J. Electrochem. Soc.* **158**(3), B313 (2011). <https://doi.org/10.1149/1.3530796>
- T. Binninger, E. Fabbri, R. Kotz, T.J. Schmidt, Determination of the electrochemically active surface area of metal-oxide supported platinum catalyst. *J. Electrochem. Soc.* **161**(3), H121–H128 (2013). <https://doi.org/10.1149/2.055403jes>
- G. Jerkiewicz, G. Vatankhah, J. Lessard, M.P. Soriaga, Y.S. Park, Surface-oxide growth at platinum electrodes in aqueous H₂SO₄ Reexamination of its mechanism through combined cyclic-voltammetry, electrochemical quartz-crystal Nanobalance, and Auger electron spectroscopy measurements. *Electrochim. Acta* **49**(9–10), 1451–1459 (2004). <https://doi.org/10.1016/j.electacta.2003.11.008>
- G. Jerkiewicz, G. Vatankhah, S.I. Tanaka, J. Lessard, Discovery of the potential of minimum mass for platinum electrodes. *Langmuir* **27**(7), 4220–4226 (2011). <https://doi.org/10.1021/la200153n>
- B.K. Matsutani, K. Hayakawa, T. Tada, Effect of particle size of platinum and platinum-cobalt catalysts on stability against load cycling. *Platin. Met. Rev* **54**(4), 223–232 (2010). <https://doi.org/10.1595/147106710X523698>
- K. Hengge, T. Gänsler, E. Pizzutilo, C. Heinzl, M. Beetz, K.J.J. Mayrhofer, C. Scheu, Accelerated fuel cell tests of anodic Pt/Ru catalyst via identical location TEM: new aspects of degradation behavior. *Int. J. Hydrog. Energy* **42**(40), 25359–25371 (2017). <https://doi.org/10.1016/j.ijhydene.2017.08.108>
- M. Wesselmarm, B. Wickman, C. Lagergren, G. Lindbergh, The impact of iridium on the stability of platinum on carbon thin-film model electrodes. *Electrochim. Acta* **111**, 152–159 (2013). <https://doi.org/10.1016/j.electacta.2013.07.108>
- N. Macauley, D.D. Papadias, J. Fairweather, D. Spornjak, D. Langlois, R. Ahluwalia, K.L. More, R. Mukundan, R.L. Borup, Carbon corrosion in PEM fuel cells and the development of accelerated stress tests. *J. Electrochem. Soc.* **165**(6), F3148–F3160 (2018). <https://doi.org/10.1149/2.0061806jes>
- S.J. Lee, S. Mukerjee, E.A. Ticianelli, J. McBreen, Electrocatalysis of CO tolerance in hydrogen oxidation reaction in PEM fuel cells. *Electrochim. Acta* **44**(19), 3283–3293 (1999). [https://doi.org/10.1016/S0013-4686\(99\)00052-3](https://doi.org/10.1016/S0013-4686(99)00052-3)
- T. Lopes, V.A. Paganin, E.R. Gonzalez, The effects of hydrogen sulfide on the polymer electrolyte membrane fuel cell anode catalyst: H₂S–Pt/C interaction products. *J. Power Sources* **196**(15), 6256–6263 (2011). <https://doi.org/10.1016/j.jpowsour.2011.04.017>
- H. Angerstein-Kozłowska, B.E. Conway, W.B.A. Sharp, The real condition of electrochemically oxidized platinum surfaces. *Electroanal. Chem. Interfacial Electrochem.* **43**(1), 9–36 (1973)
- H. Angerstein-Kozłowska, B.E. Conway, B. Barnett, J. Mozota, The role of ion adsorption in surface oxide formation and reduction at noble metals: general features of the surface process. *J. Electroanal. Chem.* **100**(1–2), 417–446 (1979)
- D. Pletcher, S. Sotiropoulos, Hydrogen adsorption-desorption and oxide formation-reduction on polycrystalline platinum in unbuffered aqueous solutions. *J. Chem. Soc. Faraday Trans.* **90**(24), 3663–3668 (1994). <https://doi.org/10.1039/FT9949003663>
- S.G. Rinaldo, W. Lee, J. Stumper, M. Eikerling, Mechanistic principles of platinum oxide formation and reduction. *Electrocatalysis* **5**(3), 262–272 (2014). <https://doi.org/10.1007/s12678-014-0189-y>
- E.L. Redmond, B.P. Setzler, F.M. Alamgir, T.F. Fuller, Elucidating the oxide growth mechanism on platinum at the cathode in PEM fuel cells. *Phys. Chem. Chem. Phys.* **16**(11), 5301–5311 (2014). <https://doi.org/10.1039/c3cp54740j>
- M.D. Edmundson, F.C. Busby, Overcoming artifacts in cyclic voltammetry through the use of multiple scan rates and potential windows. *ECS Trans. Electrochem. Soc.* **41**(1), 661–671 (2011). <https://doi.org/10.1017/CBO9781107415324.004>
- R.N. Carter, S.S. Kocha, F. Wagner, M. Fay, H.A. Gasteiger, Artifacts in measuring electrode catalyst area of fuel cells through cyclic voltammetry. *ECS Trans.* **11**(1), 403–410 (2007). <https://doi.org/10.1149/1.2780954>
- T. Biegler, D.A.J. Rand, R. Woods, Limiting oxygen coverage on platinumized platinum; relevance to determination of real platinum area by hydrogen adsorption. *J. Electroanal. Chem.* **29**(2), 269–277 (1971). [https://doi.org/10.1016/S0022-0728\(71\)80089-X](https://doi.org/10.1016/S0022-0728(71)80089-X)
- A. Kongkanand, M.F. Mathias, The priority and challenge of high-power performance of low-platinum proton-exchange membrane fuel cells. *J. Phys. Chem.* **7**(7), 1127–1137 (2016). <https://doi.org/10.1021/acs.jpcclett.6b00216>
- K. Eom, G. Kim, E. Cho, J.H. Jang, H.-J. Kim, S.J. Yoo, S.-K. Kim, B.K. Hong, Effects of Pt loading in the anode on the durability of a membrane-electrode assembly for polymer electrolyte membrane fuel cells during startup/shutdown cycling. *Int. J. Hydrog. Energy* **37**(23), 18455–18462 (2012)
- Y. Hashimasa, Y. Matsuda, M. Akai, Effects of platinum loading on PEFC power generation performance deterioration by carbon monoxide in hydrogen fuel. *ECS Trans.* **26**(1), 131–142 (2010). <https://doi.org/10.1149/1.3428984>
- S. Prass, K.A. Friedrich, N. Zamel, Tolerance and recovery of ultralow-loaded platinum anode electrodes upon carbon monoxide and hydrogen sulfide exposure. *Molecules* **24**(19), 1–14 (2019). <https://doi.org/10.3390/molecules24193514>
- B.K. Hong, P. Mandal, J.G. Oh, S. Litster, On the impact of water activity on reversal tolerant fuel cell anode performance and durability. *J. Power Sources* **328**, 280–288 (2016). <https://doi.org/10.1016/j.jpowsour.2016.07.002>
- X. Zhou, H. Ji, B. Li, C. Zhang, High-repetitive reversal tolerant performance of proton-exchange membrane fuel cell by designing a suitable anode. *ACS Omega* **5**(17), 10099–10105 (2020). <https://doi.org/10.1021/acsomega.0c00638>

29. S. Tahmasebi, A.A. McMath, J. van Drunen, G. Jerkiewicz, Catalytic duality of platinum surface oxides in the oxygen reduction and hydrogen oxidation reactions. *Electrocatalysis* **8**(4), 301–310 (2017). <https://doi.org/10.1007/s12678-017-0372-z>
30. Y. Zhao, X. Li, J.M. Schechter, Y. Yang, Revisiting the oxidation peak in the cathodic scan of the cyclic voltammogram of alcohol oxidation on noble metal electrodes. *RSC Adv.* **6**(7), 5384–5390 (2016). <https://doi.org/10.1039/c5ra24249e>
31. T. Unmüssig, J. Melke, A. Fischer, Synthesis of Pt@TiO₂ nanocomposite electrocatalysts for enhanced methanol oxidation by hydrophobic nanoreactor templating. *Phys. Chem. Chem. Phys.* **21**(25), 13555–13568 (2019). <https://doi.org/10.1039/c9cp00502a>
32. R. Manoharan, J.B. Goodenough, Methanol oxidation in acid on ordered NiTi. *J. Mater. Chem.* **2**(8), 875–887 (1992). <https://doi.org/10.1039/jm9920200875>
33. A.M. Hofstead-Duffy, D.J. Chen, S.G. Sun, Y.J. Tong, Origin of the current peak of negative scan in the cyclic voltammetry of methanol electro-oxidation on Pt-based electrocatalysts: a revisit to the current ratio criterion. *J. Mater. Chem.* **22**(11), 5205–5208 (2012). <https://doi.org/10.1039/c2jm15426a>
34. E. Passalacqua, P.L. Antonucci, M. Vivaldi, A. Patti, V. Antonucci, N. Giordano, K. Kinoshita, The influence of Pt on the electrooxidation behaviour of carbon in phosphoric acid. *Electrochim. Acta* **37**(15), 2725–2730 (1992). [https://doi.org/10.1016/0013-4686\(92\)85199-U](https://doi.org/10.1016/0013-4686(92)85199-U)
35. K. Kinoshita, J.A.S. Bett, Potentiodynamic analysis of surface oxides on carbon blacks. *Carbon* **N. Y.** **11**(4), 403–411 (1973). [https://doi.org/10.1016/0008-6223\(73\)90080-8](https://doi.org/10.1016/0008-6223(73)90080-8)
36. S.C. Ball, S.L. Hudson, D. Thompsett, B. Theobald, An investigation into factors affecting the stability of carbons and carbon supported platinum and platinum/cobalt alloy catalysts during 1.2 V potentiostatic hold regimes at a range of temperatures. *J. Power Sources* **171**(1), 18–25 (2007). <https://doi.org/10.1016/j.jpowsour.2006.11.004>
37. S. Maass, F. Finsterwalder, G. Frank, R. Hartmann, C. Merten, Carbon support oxidation in PEM fuel cell cathodes. *J. Power Sources* **176**(2), 444–451 (2008). <https://doi.org/10.1016/j.jpowsour.2007.08.053>
38. J. Willsau, J. Heitbaum, The influence of Pt-activation on the corrosion of carbon in gas diffusion electrodes—a Dems study. *J. Electroanal. Chem.* **161**(1), 93–101 (1984). [https://doi.org/10.1016/S0022-0728\(84\)80252-1](https://doi.org/10.1016/S0022-0728(84)80252-1)
39. A. Pandey, Z. Yang, M. Gummalla, V.V. Atrazhev, N.Y. Kuzminykh, V.I. Sultanov, S. Burlatsky, A carbon corrosion model to evaluate the effect of steady state and transient operation of a polymer electrolyte membrane fuel cell. *J. Electrochem. Soc.* **160**(9), F972–F979 (2013). <https://doi.org/10.1149/2.036309jes>
40. L. Castanheira, W.O. Silva, F.H.B. Lima, A. Crisci, L. Dubau, F. Maillard, Carbon corrosion in proton-exchange membrane fuel cells: effect of the carbon structure, the degradation protocol, and the gas atmosphere. *ACS Catal.* **5**(4), 2184–2194 (2015). <https://doi.org/10.1021/cs501973j>
41. Y. Yamashita, S. Itami, J. Takano, K. Kakinuma, H. Uchida, M. Watanabe, A. Iiyama, M. Uchida, Degradation mechanisms of carbon supports under hydrogen passivation startup and shutdown process for PEFCs. *J. Electrochem. Soc.* **164**(4), F181–F187 (2017). <https://doi.org/10.1149/2.0101704jes>
42. H. Kumpulainen, T. Peltonen, U. Koponen, M. Bergelin, M. Valkiainen, M. Wasberg, In situ voltammetric characterization of PEM fuel cell catalyst layers. *VTT Tied. - Valt. Tek. Tutkimusk.* 3–28 (2002)
43. B.K. Kakati, A.R.J. Kucernak, Gas phase recovery of hydrogen sulfide contaminated polymer electrolyte membrane fuel cells. *J. Power Sources* **252**, 317–326 (2014). <https://doi.org/10.1016/j.jpowsour.2013.11.077>
44. Y. Hang Li, J. Xing, Z. Jia Chen, Z. Li, F. Tian, L. Rong Zheng, H. Feng Wang, P. Hu, H. Jun Zhao, H. Gui Yang, Unidirectional suppression of hydrogen oxidation on oxidized platinum clusters. *Nat. Commun.* **4**(1), 1–7 (2013). <https://doi.org/10.1038/ncomms3500>
45. J. Jiang, A. Kucernak, Investigations of fuel cell reactions at the composite microelectrode | solid polymer electrolyte Interface. I. Hydrogen oxidation at the nanostructured Pt | Nafion® membrane Interface. *J. Electroanal. Chem.* **567**(1), 123–137 (2004). <https://doi.org/10.1016/j.jelechem.2003.12.018>
46. N.M. Marković, S.T. Sarraf, H.A. Gasteiger, P.N. Ross, Hydrogen electrochemistry on platinum low-index single-crystal surfaces in alkaline solution. *J. Chem. Soc. Faraday Trans.* **92**(20), 3719–3725 (1996). <https://doi.org/10.1039/FT9969203719>
47. M.K. Kundu, T. Bhowmik, R. Mishra, S. Barman, Platinum nanostructure / nitrogen-doped carbon hybrid: enhancing its base media HER / HOR activity through bi- functionality of the catalyst. *ChemSusChem* **11**(14), 2388–2401 (2018). <https://doi.org/10.1002/cssc.201800856>
48. H. Iden, S. Takaichi, Y. Furuya, T. Mashio, Y. Ono, A. Ohma, Relationship between gas transport resistance in the catalyst layer and effective surface area of the catalyst. *J. Electroanal. Chem.* **694**, 37–44 (2013). <https://doi.org/10.1016/j.jelechem.2013.02.008>
49. L. Wang, A. Roudgar, M. Eikerling, Ab initio study of stability and site-specific oxygen adsorption energies of Pt. *J. Phys. Chem. C* **113**(42), 17989–17996 (2009). <https://doi.org/10.1021/jp900965q>

Publisher's Note Springer Nature remains neutral with regard to jurisdictional claims in published maps and institutional affiliations.